Representative diatom and coccolithophore species exhibit divergent responses throughout simulated upwelling cycles

Robert H. Lampe[1,2], Gustavo Hernandez[2], Yuan Yu Lin[3], and Adrian Marchetti[2,✉]

[1]Integrative Oceanography Division, Scripps Institution of Oceanography, University of California, San Diego, La Jolla, CA, USA
[2]Department of Marine Sciences, University of North Carolina at Chapel Hill, Chapel Hill, NC, USA

Phytoplankton communities in upwelling regions experience a wide range of light and nutrient conditions as a result of upwelling cycles. These cycles can begin with a bloom at the surface followed by cells sinking to depth when nutrients are depleted. Cells can then be transported back to the surface with upwelled waters to seed another bloom. In spite of the physicochemical extremes associated with these cycles, diatoms consistently outcompete other phytoplankton when upwelling events occur. Here we simulated the conditions of a complete upwelling cycle with a common diatom, *Chaetoceros decipiens*, and coccolithophore, *Emiliania huxleyi*. We show that while both organisms exhibited physiological and transcriptomic plasticity, the diatom displayed a distinct response enabling it to rapidly shift-up growth and nitrate assimilation when returned to light and nutrients. As observed in natural diatom communities, *C. decipiens* frontloads key transcriptional and nitrate assimilation genes coordinating its rapid response. Low iron simulations showed that *C. decipiens* is capable of maintaining this response when iron is limiting whereas *E. huxleyi* could not. Differential expression between iron treatments further revealed molecular mechanisms used by each organism under low iron availability. Overall, these results highlight the responses of two dominant phytoplankton groups to upwelling cycles, providing insight into the mechanisms fueling diatom success during upwelling events in current and future oceans.

Correspondence: ***amarchetti@unc.edu***

Introduction

Phytoplankton communities in coastal upwelling regions disproportionately contribute to global primary production and serve as the base of highly productive food chains (1). Within these environments, phytoplankton undergo a cycle in which subsurface populations are vertically transported with upwelled water masses to seed surface blooms and return to depth as upwelling subsides and nutrients are depleted (2). Surviving cells at depth may act as seed stocks when upwelling returns, and the cells are once again transported upwards with nutrient-rich waters. Herein this loop is referred to as the upwelling conveyer belt cycle (UCBC; Fig. 1).

The physiological response of phytoplankton to the upwelling portion of the UCBC is referred to as the shift-up response and includes an acceleration of processes such as nitrate uptake, assimilation, and growth (3, 4). Based on field observations, diatoms are believed to be particularly suited for shift-up leading to their dominance of phytoplankton blooms following upwelling (2, 5, 6). When upwelling delivers cells and nutrients into well-lit surface waters, diatoms quickly respond to available nitrate and increase their nitrate uptake rates compared to other phytoplankton groups allowing them to bloom (7). This phenomenon may partially be explained by frontloading nitrate assimilation genes, i.e. high expression before the upwelling event occurs, in addition to diatom's unique metabolic integration of nitrogen and carbon metabolic pathways (6, 8).

Coupled to rapid nitrate uptake rates, phytoplankton in natural communities have been observed to dramatically alter their carbon-to-nitrogen (C:N) ratios (6, 7, 9). C:N ratios well above the predicted Redfield value (6.6:1) imply that the cells faced nitrogen limitation as the upwelled waters aged, and then the cells sank to depth, but this alteration has yet to be shown in the context of a complete UCBC cycle and without the influence of other non-phytoplankton detrital material which would affect these measurements (6, 7, 9). Ultimately, such shifts in cellular elemental quotas associated with sinking cells can decouple the biogeochemical cycling of these elements.

The responses of phytoplankton within the UCBC are also influenced by the availability of the micronutrient iron. In the California and Peru/Humboldt Upwelling Zones for example, iron delivery is primarily dependent on riverine input and upwelling-driven resuspension of continental shelf sediments (10–14). In areas with steep continental shelves, reduced interaction between upwelled waters and sediment can result in decreased iron relative to macronutrients resulting in iron limitation as the phytoplankton bloom develops. As upwelling is anticipated to intensify from climate change (15), increased upwelled nitrate has the potential to be further unmatched by upwelled iron causing an expansion of iron limitation regions (1). Furthermore, ocean acidification may result in reduced iron bioavailability to phytoplankton (16, 17).

An understanding of phytoplankton responses to the UCBC remains limited and is primarily based on a relatively small collection of field studies focused on the shift-up response resulting in no complete view of the cycle (2, 7). Importantly, differences in responses among phytoplankton groups influences both the community structure and biogeochemical cycling in upwelling areas which may be altered by iron limitation (1). Using a combined physiological and

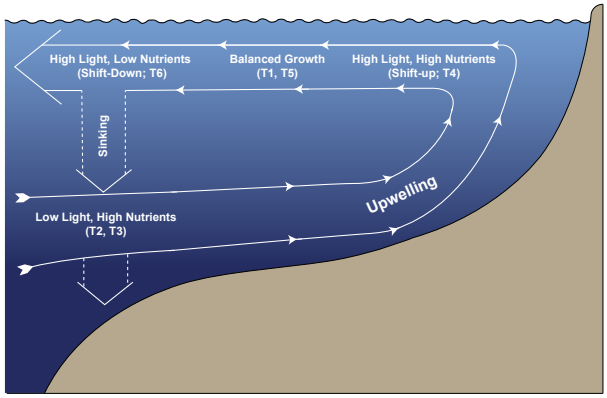

Fig. 1. Conceptual overview of the upwelling conveyer belt cycle (UCBC) reproduced from Wilkerson and Dugdale (4) and annotated with experimental time points.

Table 1. Description of experimental time points.

Name	Latitude
1	Mid-exponential growth #1
2	Stationary Phase #1
	(4 d in stationary phase, 1 d in dark)
3	Stationary Phase #2
	(13 d in stationary phase, 10 d in dark)
4	12 hours after returning to light and nutrients
5	Mid-exponential growth #2
6	Stationary Phase #3
	(2 days in stationary phase, light)

transcriptomic approach, we examine the responses of phytoplankton throughout the various light and nutrient conditions associated with the UCBC via culture-based simulations. Samples were collected with higher resolution surrounding the upwelling portion of the UCBC to evaluate the ability to exhibit a shift-up respone. In order to compare two phytoplankton lineages commonly present in upwelled waters, a representative diatom, *Chaetoceros decipiens*, and coccolithophore, *Emiliania huxleyi*, were used; both isolates were obtained from the California Upwelling Zone. The genus *Chaetoceros* is considered the most abundant and diverse diatom genus and is highly prevalent in the California coastal waters (18, 19). *E. huxleyi* is a globally distributed dominant bloom-forming coccolithophore and found to be one of the most abundant coccolithophores within a coastal California time series (20–22). Together, this comparison highlights changes in phytoplankton C:N ratios which influence biogeochemical cycling of these elements and examines unique physiological and molecular responses that provide insight into diatom blooms in upwelling regions.

Materials and Methods

Experimental design. Two phytoplankton species isolated from the California Upwelling Zone were used in this study: a diatom, *Chaetoceros decipiens* (UNC1416), and a coccolithophore, *Emiliania huxleyi* (UNC1419). Species isolation and identification are described in Lampe et al. (6). Cultures were grown in artificial Aquil* medium following trace metal clean (TMC) techniques at 12°C and approximately 115 µmol photons m^{-2} s^{-1} (23–25). Starting macronutrient concentrations were modified from standard Aquil* such that nitrate rather than silicate would be drawn down and depleted first by diatoms (50 µmol L^{-1} NO_3, 10 µmol L^{-1} PO_4, 200 µmol L^{-1} H_4SiO_4). Aquil was chelexed in a TMC room, microwave sterilized, allowed to cool, and then supplemented with filter-sterilized (0.2 µm Acrodisc®) EDTA-trace metals (minus iron) and vitamins (B12, thiamine, and biotin). Trace metals were buffered using 100 µmol L^{-1} EDTA and added at the concentrations listed in Sunda et al. (25) except Cd which was added at a total concentration of 121 nmol L^{-1}. Premixed Fe-EDTA (1:1) was added separately at a total concentration of 1370 nmol L^{-1} for the high iron treatments or 3.1 nmol L^{-1} for the low iron treatments. The resulting concentrations of iron not complexed to EDTA (Fe') were estimated as 2730 pmol L^{-1} (high iron) and 6 pmol L^{-1} (low iron)(25) resulting in Fe-replete and Fe-limited growth, respectively. Vitamins were added at f/2 concentrations. Media were allowed to equilibrate overnight before use.

Cultures were acclimated to medium using the semi-continuous batch culture technique at the two iron concentrations in acid-cleaned 28 mL polycarbonate centrifuge tubes with stable growth rates (26). Cultures were then grown in a 1 L polycarbonate bottle, and when in exponential phase, 5 mL (high iron) or 20 mL (low iron) of each culture were then transferred to triplicate clean 2 L polycarbonate bottles fitted with Teflon tubing for subsampling and bubbling. Seawater was gently stirred and continuously bubbled with air passed through 1.2 mol L^{-1} HCl then TMC Milli-Q before the culture bottle. Cultures were not axenic although sterile techniques were used for all culture work to minimize contamination.

The upwelling conveyer belt cycle (UCBC) was simulated by growing or transitioning the cultures to varying light and nutrient conditions (Fig. 1, Table 1). First, to simulate bloom and termination phases, cultures were grown in exponential phase until nutrient exhaustion, at which time cells entered stationary phase. After three days in stationary phase, bubbling and stirring were halted and the bottles were moved to a dark (0 µmol photons m^{-2} s^{-1}) incubator to simulate sinking out of the euphotic zone. Although nutrient concentrations would likely increase in deeper waters in the natural environment, cells were maintained in nitrate-depleted medium during this stage. After 10 days, 500 mL of culture was transferred into 1.5 L of fresh medium and returned to the light with stirring and bubbling resumed. The 10 day time frame was selected based on satellite observations of timing between upwelling (6) and as a point at which differences in lag time to return to exponential growth were observed between species (Fig. S1)(6). Cultures were subsequently grown until stationary growth was measured for two days, thus completing the cycle. Subsampling was performed by first dispensing into sterilized bottles under a laminar flow hood in a TMC room, then aliquoting from this sample. Relative abundances and growth throughout the experiment were assessed by regular measurements of blank-corrected raw flu-

orescence units (RFUs) with a Turner 10-AU fluorometer. Additional materials and methods are available in the Supplementary Information.

Gene Expression Analysis. RNA libraries for the UCBC simulations were constructed using a custom protocol for 3' poly-A-directed mRNA-seq (also known as TagSeq) based on Meyer et al. (27) and adapted for Illumina HiSeq based on Lohman et al. (28) and Strader et al. (29) (Supplementary Materials and Methods). PCR duplicates were removed based on a matching degenerate leader sequence incorporated during cDNA synthesis and a match of the first 20 bases as described by Dixon et al. (30). Reads were trimmed for adapter removal and quality with a minimum length of 20 bases with Trimmomatic v0.38 (31). Transcripts were quantified with Salmon v0.9.1 with the GC bias correction option against reference transcriptomes generated from the same strains (32) (Supplementary Materials and Methods). Normalized counts, fold change values, and associated Benjamini & Hochberg adjusted p-values were calculated with DESeq2 v1.22.2 (33). Reference transcriptome and experimental results are further detailed in Datasets S1, S2, and S3.

Correlation network analysis of gene expression was performed using WGCNA using variance-stabilizing transformed counts generated by DESeq2 as input (34). Samples from both the high and low iron treatments were used for analysis. Contigs with fewer than 10 normalized counts in more than 90% of the samples were removed before analysis. A signed adjacency matrix was constructed for each organism using a soft-thresholding power of 14 for the *C. decipiens* samples and 22 for the *E. huxleyi* samples (Fig. S2). The soft-thresholding power was selected as the lowest power that satisfies the approximate scale-free topology criteria as described by Langfelder and Horvath (34). The adjacency matrix was then transformed into a Topological Overlap Matrix (TOM). Subnetworks, or modules, were created by hierarchical clustering of the TOM with the following parameters: minModuleSize = 30, deepSplit = 2. The grey module is reserved for genes that are not assigned to a module. The first principal component of each module, i.e. eigengene, was correlated (Pearson) with each time point and associated p-values were calculated. Contigs in modules that were significant for a specific time point were then also correlated (Pearson) to the same time points to evaluate significance on an individual contig basis. The corresponding p-values were corrected for multiple testing using the Benjamini & Hochberg false discovery rate controlling procedure (35).

Statistical Analyses. One- and two-way ANOVAs followed by Tukey's multiple comparison test were performed on the biological and chemical properties of the seawater media in Graphpad PRISM v8.3.0.

Data deposition. Raw reads for the *C. decipiens* and *E. huxleyi* experiments are deposited in the National Center for Biotechnology Information (NCBI) Sequence Read Archive (SRA) under the accession nos. SRP176464 and SRP178167 (Bioproject accession nos. PRJNA513340 and PRJNA514092) respectively. Raw reads for the reference transcriptomes are also deposited in SRA under the accession nos. SRP234548 and SRP234650 (Bioproject accession nos. PRJNA593314 and PRJNA593538). Assemblies and annotations for each reference transcriptome are deposited in Zenodo (doi:10.5281/zenodo.3747717 and doi:10.5281/zenodo.3747989).

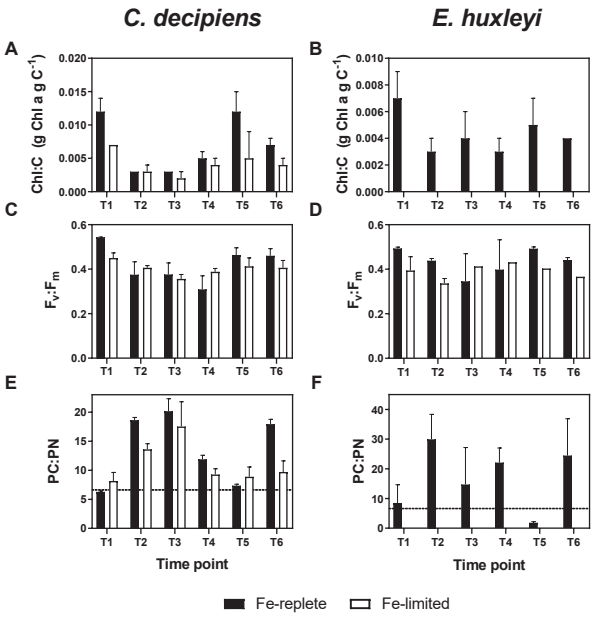

Fig. 2. Biochemical and photophysiological measurements for *C. decipiens* and *E. huxleyi* in the Fe-replete (black) and Fe-limited (white) UCBC simulations: (A, B) Chlorophyll *a* to carbon ratios (g Chl *a* g C^{-1}). (C, D) Maximum photochemical yields of photosystem II (F_v:F_m). (E, F) Particulate carbon to particulate nitrogen ratios. The dashed line indicates the Redfield C:N ratio (106:16). Error bars indicate the standard deviation of the mean (n = 3). Data are not available in *E. huxleyi* for chlorophyll *a* and for PC:PN at all time points in the Fe-limited cultures.

Results and Discussion

Physiological and transcriptomic responses throughout the UCBC. *C. decipiens* and *E. huxleyi* displayed clear physiological responses to the different UCBC conditions under iron-replete conditions (Fig. 2; black bars). Both significantly reduced chlorophyll *a* under stationary growth phases ($P < 0.05$)(Figs. 2A and 2B). Photosynthetic efficiency (F_v:F_m) was also lower in stationary phase time points compared to the initial exponential growth time point (Figs. 2C and 2D). In *C. decipiens*, these declines were significant ($P < 0.001$). Following the dark period, both species increased photosynthetic efficiency when the cells returned to exponential growth which is consistent with previous field observations (6).

Cellular particulate C:N ratios for both species also fluctuated throughout the cycle (Figs. 2E and 2F). Both species were growing near Redfield-predicted values (6.6:1) during the initial exponential growth phase and increased their C:N ratios during stationary phase following N depletion. As with chlorophyll and F_v:F_m in *C. decipiens*, these differences were highly significant ($P < 0.0001$). Previous field observations of particulate C:N from phytoplank-

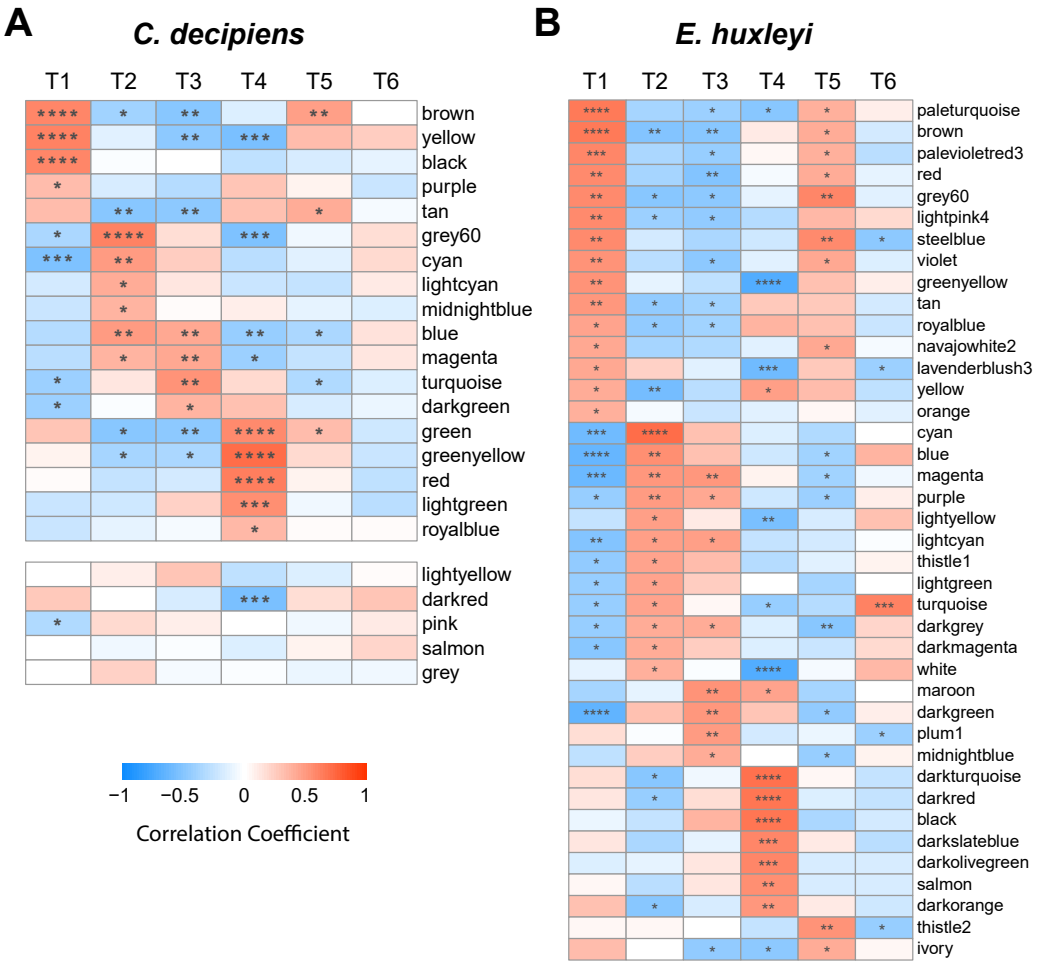

Fig. 3. WGCNA module-time point correlations (Pearson) for (A) *C. decipiens* and (B) *E. huxleyi* at the time points throughout the UCBC. Significance in correlation is shown within each cell as follows: *P $\leq$ 0.05, **P $\leq$ 0.01, ***P $\leq$ 0.001, ****P $\leq$ 0.0001. Row names indicate WGCNA modules. Modules with no postitive significant correlations are shown separated in panel A for *C. decipiens* and in Fig. S3 for *E. huxleyi*.

Table 2. The number of KEGG Orthologs and protein families (Pfam) that were significantly associated with *C. decipiens*, *E. huxleyi*, or both (shared) by WGCNA at each time point.

		T1	T2	T3	T4	T5	T6
KEGG	Shared	66	22	4	109	14	N/A
Ortholog	*C. decipiens*	209	122	354	454	44	N/A
	E. huxleyi	512	300	95	470	221	98
Pfam	Shared	100	44	23	142	16	N/A
	C. decipiens	199	95	279	379	47	N/A
	E. huxleyi	489	319	94	412	219	148

ton communities at depth have also shown values far exceeding the Redfield ratio reaching as high as 60:1, although uncertainty remained as to whether these results were a result of cellular modifications or simply C-rich detrital material (6, 7, 9). With a maximum C:N of 20.2 ± 2.1 for *C. decipiens* and 29.96 ± 8.4 for *E. huxleyi* under the iron-replete condition, it can be inferred that a large proportion of the high carbon relative to nitrogen can be attributed to cells suffering from N and/or light limitation. Similarly under N-limitation, several *Thalassiosira* species were shown to have C:N ratios over 20 which can be attributed to an accumulation of carbohydrates (36). Previous laboratory experiments that mimicked sinking cells with the diatom *Pseudo-nitzschia australis* grown in excess N relative to Si did not show as dramatic of an increase in C:N suggesting that Si limitation, as can often occur in conjunction with Fe-limited diatoms in the California coastal upwelling region, may influence these elemental stoichiometries (37, 38).

To examine gene expression profiles in both organisms throughout the UCBC, transcriptome-wide co-expression was analyzed with Weighted Gene Co-Expression Network Analysis (WGNCA). WGCNA resulted in 23 modules (clus-

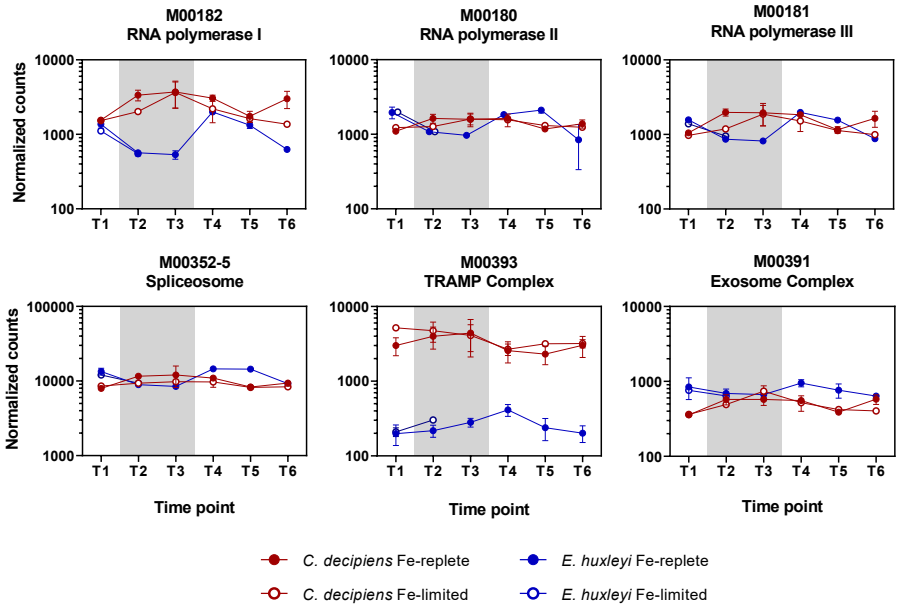

Fig. 4. Summed normalized counts assigned to select transcription-related KEGG modules (M) in *C. decipiens* (red) and *E. huxleyi* (blue) under Fe-replete (closed circles) and Fe-limited (open circles) treatments. Error bars indicate the standard deviation of the mean (n = 3).

ters of interconnected genes) for *C. decipiens* and 58 modules for *E. huxleyi*. Significant positive correlations (Pearson; $p < 0.05$) between modules and all time points apart from T6 for *C. decipiens* were found indicating that there is distinct and coordinated expression of certain genes within each UCBC stage for both organisms (Figs. 3 and S3). Several modules were significantly associated with the time point pairs that represented similar environmental conditions (T1 and T5; T2 and T3). Eighteen modules in *C. decipiens* and forty modules in *E. huxleyi* had significant positive correlations with each time point. Importantly, these significant associates were largely different between time points indicating that both organisms exhibited a high degree of transcriptional plasticity in response to the different UCBC conditions.

Genes associated with each UCBC stage were identified by querying contigs significantly correlated with a time point within modules that were also significantly correlated with that time point (Datasets S4 and S5). By comparing KEGG orthologs (KOs) and protein family (Pfam) annotations of contigs associated at each time point, similarities or differences in expression for both organisms throughout the UCBC were examined. Overall, *C. decipiens* and *E. huxleyi* showed highly divergent responses throughout the UCBC with 1199 KOs and 1028 protein families significantly associated with *C. decipiens* time points and 1505 KOs and 1348 protein families significantly associated with *E. huxleyi* time points. Only 513 KOs and 518 protein families were significantly associated at a time point in both species. Furthermore, these were largely not associated with the same time points in both organisms. At each time point, more KOs or protein families were significantly associated with one of the organisms rather than both (Table 2).

Broadly, this divergence in responses represents differing metabolic investments and potential niche partitioning between diatoms and coccolithophores; however, some similarities can be observed by examining specific KEGG orthologs, KEGG modules, and protein families associated with each organism at each time point (Datasets S4 and S5). In both organisms, many photosynthesis related genes were associated with time points when light was available. Expression of glycolysis and fatty acid biosynthesis genes during exponential growth was also common. At 12 hours after returning to the light, both highly expressed genes associated with translation and amino acid biosynthesis as they resumed growth.

However, WGCNA revealed an important difference in the timing of gene expression related to transcription (Fig. 4). These include RNA polymerases and spliceosome genes to generate mature RNA, and TRAMP and exosome complexes which can interact to degrade abnormal rRNAs and spliced-out introns (39). *C. decipiens* displayed elevated expression of these gene sets during stationary growth, particularly at T3. In an opposite pattern, *E. huxleyi* decreased expression of these genes during stationary phase and elevated expression at T4 in response to a return to light and nutrients. WGNCA indicated that these gene sets were significantly associated with T3 in *C. decipiens* but with T4 in *E. huxleyi* (Datasets S4 and S5).

These opposing patterns indicate relatively high cellular investments in transcription during opposite conditions. In *C. decipiens*, this higher expression corresponds to periods when conditions are not optimal for growth, i.e. a lack of light and nutrients, whereas higher expression corresponds to opposite conditions in *E. huxleyi*. This observation is not unlike previous ones of these phytoplankton groups in the field where diatoms were found to highly express nitrogen assimilation genes prior to optimal growth conditions (6). This transcriptional investment is termed frontloading and may enable diatoms to outcompete other groups by being transcriptionally proactive rather than reactive in response to frequent changes in environmental conditions (40).

The shift-up response and nitrogen assimilation. Beyond transcription gene sets, frontloading of nitrogen assimilation genes and an acceleration of nitrate uptake, i.e. the shift-up response, is hypothesized to be linked to diatom success during the upwelling portion of the UCBC (3, 4, 7). As a result, the upwelling portion of the UCBC simulation was sampled after 12 hours (T4) to investigate the physiological capability for relatively rapid shift-up. By comparing T3 through T5, a view from pre-upwelling, 12 hours after upwelling, and a return to exponential growth can be examined (Fig. 1).

A rapid shift-up response was observed in *C. decipiens* compared to *E. huxleyi*. *C. decipiens* returned to exponential growth within 24 hours of returning to light and nutrients whereas *E. huxleyi* did not respond appreciably for approximately 48 hours (Fig. S1). Concurrently, the C:N ratio in *C. decipiens* rapidly declined from 20.18 ± 2.13 to 11.89 ± 0.70 within the first 12 hours of returning to light and nutrients (Figs. 2E and 2F) suggesting that *C. decipiens* rapidly assimilated nitrate once returned to optimal growth conditions. After 36 hours in the light, cellular C:N in *C. decipiens* returned to the Redfield ratio. In contrast, *E. huxleyi* maintained a high C:N ratio (22.10 ± 4.91) after returning to light for 12 hours, but the C:N ratio dramatically declined to 1.80 ± 0.40 at 3 days after returning to the light when the cells reached exponential growth (Figs. 2F and S1). This initial lack of decline indicates that *E. huxleyi* has a slower response to the newly available nitrate compared to *C. decipiens*; however, once the cells reach exponential growth, *E. huxleyi* may exhibit luxury uptake and store excess nitrate prior to an increase in cell division as evidenced by the later decline in their C:N ratio in conjunction with the highest cellular nitrogen quotas (Fig. S4). Altogether, these results align with the relatively rapid shift-up response of diatoms compared to other phytoplankton groups, and that nitrate uptake rates are likely rapidly increasing to result in the observed changes.

Results from a field-based simulated upwelling experiment suggest that frontloading of nitrogen assimilation genes is an underlying molecular mechanism behind these responses (6). Diatoms were observed to highly express nitrate assimilation genes [nitrate transporter (*NRT*), nitrate reductase (*NR*), nitrite reductases (*NiR*)] prior to upwelling events in order to be transcriptionally proactive, i.e. frontload, in order to rapidly assimilate nitrate and outcompete other phytoplankton groups once conditions are optimal for growth.

In comparing the expression of nitrogen metabolism genes in *C. decipiens* and *E. huxleyi* from the UCBC simulation, *C. decipiens* exhibited this distinct and proactive frontloading response whereas *E. huxleyi* did not (Figs. 5A and 5B). *C. decipiens* significantly upregulated the aforementioned nitrogen assimilation genes during stationary phase ($P < 0.05$) with highest expression at 10 days in the dark, i.e. the simulated pre-upwelling condition. WGCNA also placed these genes in the blue module which was significantly associated with the dark stationary phase time points (Fig. 3, Dataset S4). Upon returning to high light and nutrients, expression of these genes significantly declined and returned to previous levels observed during exponential growth ($P < 0.01$, Fig. 4B). Diatoms also possess two nitrite reductases (Nir) both of which are localized to the chloroplast; however, one utilizes ferredoxin (Fd) and the other utilizes NAD(P)H (8). Under exponential growth, Fd-Nir transcript abundance was higher than NAD(P)H-Nir; however, under stationary growth in the light and dark, NAD(P)H-Nir transcript abundance was higher suggesting potential metabolic advantages of each nitrite reductase under these different growth conditions.

In contrast, *E. huxleyi* displayed an opposing expression pattern for their nitrate assimilation genes (Fig. 5A). During stationary growth, *E. huxleyi* significantly downregulated nitrate transporters and nitrate reductase ($P < 0.01$); nitrite reductase expression remained similar across time points. Once returned to the light and nutrients (T4), *E. huxleyi* significantly upregulated nitrate transporters ($P < 0.0001$) in response to nitrate availability and optimal growth conditions. Nitrate reductase and nitrite reductase expression also remained low throughout the experiment; therefore, in conjunction with low cellular C:N ratios, these data support that *E. huxleyi* may store nitrate for some time post-upwelling.

Unlike the nitrate assimilation genes, ammonium transporters (*AMT*) and urea transporters (*UT*) displayed a similar transcriptional pattern in both organisms; however, while nitrate transporters were among the most highly expressed nitrogen metabolism genes in *C. decipiens*, *E. huxleyi* highly expressed ammonium transporters despite ammonium not being added to the seawater medium. High expression of *AMT* and *UT* during stationary phase suggests that both organisms are tuned to exploit released ammonium and urea as nitrate was depleted, although urease expression remained low in both (Figs. 5B, 5C, and S7). *E. huxleyi* has also previously been shown to prefer ammonium over nitrate (41). The relatively high level of expression of *AMT* in *E. huxleyi* compared to *C. decipiens* corroborates this preference for ammonium and implies that the two species exhibit different nitrogen preferences.

The divergent responses between these two species with frontloading in the diatom is increasingly apparent when examining the nitrogen metabolism genes downstream of the assimilation genes, i.e. the GS-GOGAT [glutamine synthetase (*GS*) and glutamate synthase (*GOGAT*)] cycle and the ornithine-urea cycle (OUC; Figs. 5B and 5C). The GS-GOGAT cycle catalyzes ammonium into organic nitrogen. The ornithine-urea cycle (OUC) has been shown to aid the model diatom *Phaeodactylum tricornutum* in returning from N-limiting conditions by serving as a hub for nitrogen redistribution and pathway to satisfy arginine demand (8, 42). *E. huxleyi* also possesses an OUC which is hypothesized to serve a similar role (43).

In *C. decipiens*, significant differences in expression between time points were nearly absent in both the GS-GOGAT cycle under the iron-replete conditions and OUC genes under both iron treatments (Fig. 5B). These results correspond to previous field observations of constitutive and relatively high expression in diatoms pre- and post-upwelling such that

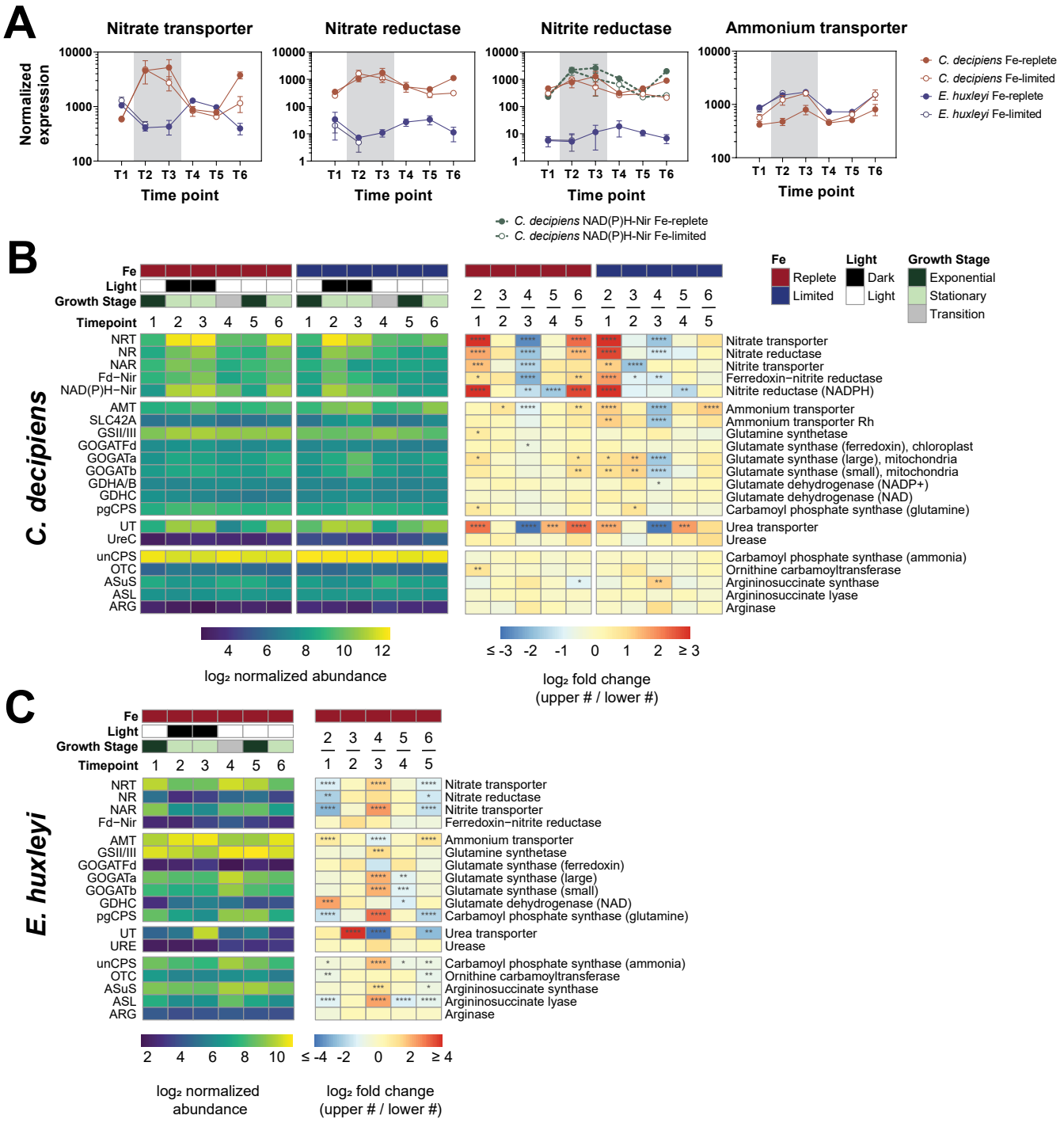

Fig. 5. Expression of nitrogen assimilation and utilization genes throughout the UCBC. (A) Line graph view of averaged nitrate assimilation and ammonium transporter normalized counts in both *C. decipiens* (red) and *E. huxleyi* (blue) under Fe-replete (closed circles) and Fe-limited conditions (open circles). *C. decipiens* possesses two nitrite reductases; therefore, Fd-Nir is shown with a solid red line and NAD(P)H-Nir is shown with a dashed green line. Error bars indicate the standard deviation of the mean (n = 3). (B) Heatmaps showing both the $\log_2$ normalized abundance and $\log_2$ fold change values throughout the UCBC. Iron status, light level, growth stage, and time point are annotated above the heatmaps where appropriate. Fold changes are compared by examining one time point to the next (later time point / earlier time point) and annotated as the upper numbered time point / the lower numbered time point. Significance in differential expression between time points is shown within each cell as follows: *P $\leq$ 0.05; **P $\leq$ 0.01; ***P $\leq$ 0.001; ****P $\leq$ 0.0001. (C) Corresponding heatmaps for *E. huxleyi* as described for panel A. Iron-limited experiments are omitted due to a lack of replication in RNA for all time points.

the cell already possesses the cellular machinery to channel assimilated nitrogen towards growth (6). Like the nitrate assimilation genes, *E. huxleyi* exhibits a different transcriptional response for the GS-GOGAT and OUC genes in response to the changing UCBC conditions. OUC genes were generally downregulated under stationary growth and upregulated in response to returning to light at T4 ($P < 0.05$). Also, in response to returning to light, *E. huxleyi* strongly upregulated GS-GOGAT genes ($P < 0.001$; Fig. 5C). Both *C. decipiens* and *E. huxleyi* displayed low and constitutive expression of arginase and urease, the final steps of the OUC pathway which similarly were not shown to exhibit a frontloading response in the same degree in the field (6). The OUC thus likely serves to satisfy demand for arginine in both organisms as predicted through metabolic flux models in *P. tricornutum* (8). Much like the nitrate assimilation genes, *C. decipiens* appears to frontload the GS-GOGAT and OUC genes whereas *E. huxleyi* exhibits a more responsive transcriptional pattern.

N-limitation has previously been studied extensively in several diatoms and *E. huxleyi* providing points of comparison. In the model pennate diatom *P. tricornutum*, genes encoding nitrate transporters, nitrate reductases, and nitrite reductases were upregulated under N limitation (44, 45), although a study examining these genes in a short-term response associated them with nitrogen replete conditions (8). Upregulation of these genes under N starvation in most cases was further shown in *Fragilariopsis cylindrus*, *Pseudo-nitzschia multiseries*, and several *Skeletonema* species (45, 46); therefore, most studies are consistent with our findings here of upregulation under N limitation suggesting that this response is shared among diatoms.

For GS-GOGAT and OUC-related genes, a pattern in gene expression is less apparent. Most studies reported changes in expression of these genes under N-replete or -deplete conditions in contrast to the lack of change observed here in *C. decipiens*, although the directionality of the expression among studies is not consistent (8, 44, 45). However, in *F. cylindrus*, *P. tricornutum*, and *P. multiseries*, stable expression of OUC genes was shown between N conditions apart from the first step, carbamoyl-phosphate synthase, similar to observations in this study (45). Therefore, unlike nitrate assimilation genes, transcriptional regulation of these genes appears to be variable among diatoms as previously suggested (45). In this case, the coordinated frontloading response of GS-GOGAT and OUC genes may be a strategy more exclusively employed by bloom-forming diatoms residing in upwelling environments.

Aligning with the results presented here, *E. huxleyi* has been shown to downregulate or show reduced activity of NRT, NR, and NiR while upregulating AMT under N-limitation, although these results are also not entirely consistent across studies (41, 43, 47–49). *E. huxleyi* also was shown to downregulate the initial OUC genes under N limitation, the one exception here being arginosuccinate synthase at T2 (43). GS-GOGAT gene expression was similarly lower in previous studies albeit not significantly different here (43).

Influences of iron limitation on UCBC responses. Iron bioavailability is an important control on phytoplankton growth in upwelling areas characterized by narrow continental shelves (1). Biogeochemical modeling of the California Current Ecosystem indicates that iron limitation is highly prevalent although only occurring at small scales and short durations relative to N limitation (50). This iron limitation occurs in both the surface mixed layer and at depth as shown with subsurface chlorophyll maximum layers (12, 51). Furthermore, projected increases in upwelled nitrate unmatched by iron coupled with ocean acidification is projected to expand iron limitation in these regions (1, 16, 17). Here UCBC simulations were performed under iron-limiting conditions to examine the effects of iron status on responses throughout the cycle.

Within the first phase of exponential growth, *C. decipiens*'s growth rate significantly declined from 0.86 d^{-1} to 0.33 d^{-1} (Fig. S1). The reduction in growth rates was comparatively smaller for *E. huxleyi* (0.73 d^{-1} to 0.64 d^{-1}). Reductions in F_v:F_m were also observed in both organisms indicating iron stress in the low iron treatments. With F_v:F_m already impacted by iron stress, the variation as a result of light and/or nitrogen stress was comparatively less to when iron was replete. Previous experiments have also suggested that *E. huxleyi* is well-suited to grow under low Fe concentrations (52). Higher growth rates may confer an advantage under low iron for *E. huxleyi* when growing in exponential phase. Yet during the UCBC, iron-limited *E. huxleyi* cells were unable to grow upon returning to light in two out of three replicates, supporting the observation that diatoms are able to outcompete coccolithophores under dynamic conditions (Fig. S1) (53).

Iron limitation can influence nitrate assimilation as the required enzymes, nitrate and nitrite reductase, can account for greater than 15 percent of the cellular iron requirement (54, 55). Iron limitation has also been shown to influence the expression of the genes that encode these proteins (56, 57). In *C. decipiens*, C:N ratios followed a similar pattern when comparing the iron-replete to iron-stressed conditions (Fig. 2). In early stationary phase (T2 and T6), cellular C:N ratios were significantly reduced, but reached similar values after 10 days in the dark. Importantly, C:N ratios in iron-limited cells still quickly approached the Redfield ratio upon returning to the light (T4) indicating that the shift-up response in N-assimilation may not be significantly impacted by low iron conditions in *C. decipiens*.

Iron limitation altered the expression levels of certain N-related genes at specific time points in *C. decipiens* (Fig. S8). The nitrate assimilation pathway was downregulated at T3 and T6. This decreased expression at T3 made expression levels between T3 and T4 similar which may explain similar responses observed pre- and post-upwelling in the field-based incubations where iron stress in the initial community was possible (6).

Genes encoding ammonium and urea transporters as well as urease were upregulated under low iron as expected with nitrate assimilation being impacted. Under low iron,

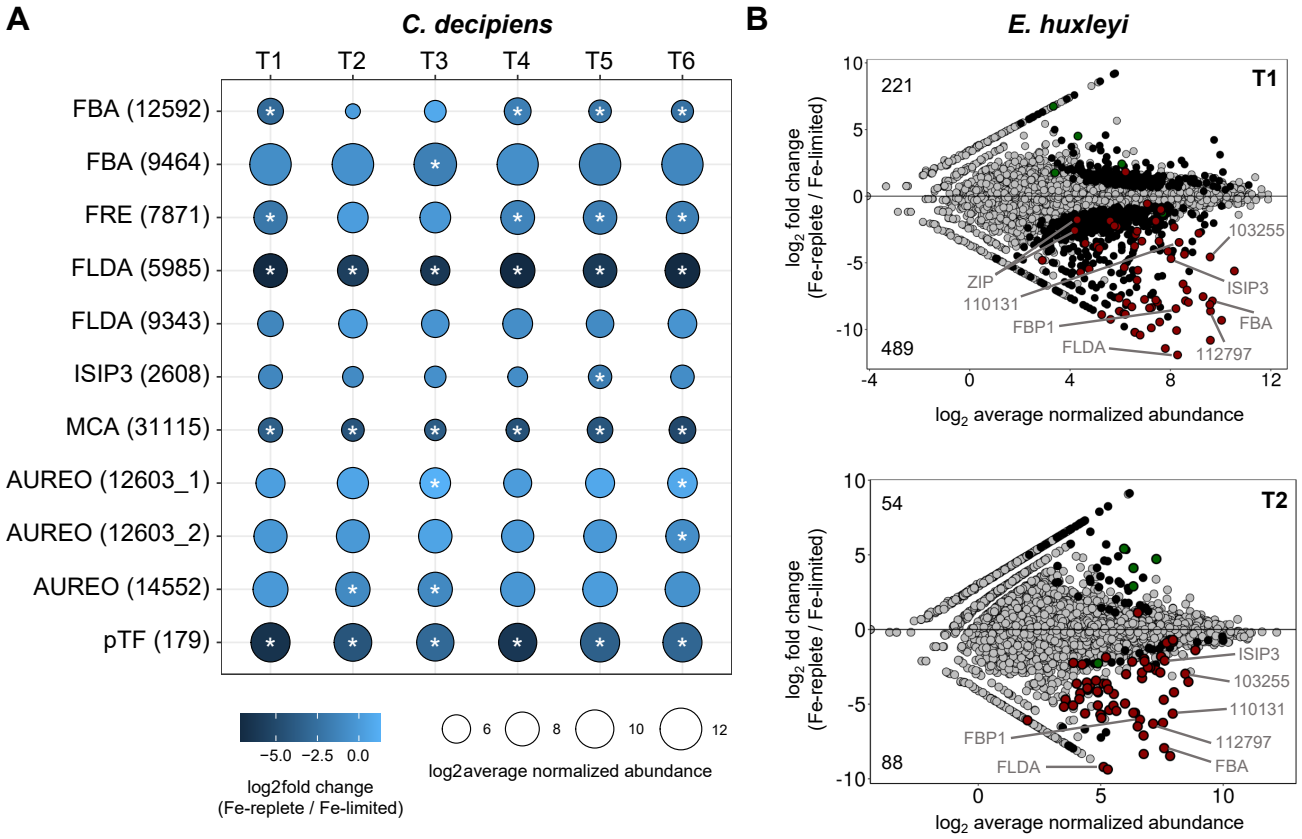

Fig. 6. Iron-related gene expression. (A) Selected genes in *C. decipiens*. Genes with contig IDs in parentheses are shown on the vertical axis. Time points are shown on the horizontal axis. Circle size and color correspond to the $\log_2$ average normalized abundance and the $\log_2$ fold change as shown in the legend. Contigs that were significantly upregulated under iron-limiting conditions are denoted with an asterisk ($P < 0.05$). Genes are abbreviated as follows: FBA fructose-bisphosphate aldolase, FRE ferric reductase, FLDA flavodoxin, ISIP3 iron-starvation induced protein 3, MCA metacaspase, AUREO aureochrome, pTF phytotransferrin. (B) MA plots showing differentially expressed contigs in *E. huxleyi* between Fe treatments at T1 (top) and T2 (bottom). Contigs are colored to denote differences in significant expression ($P < 0.05$): gray is not significant at the displayed time point, black is significant at the displayed time point but not in the other, green is significant in both with a positive fold change in the other time point, and red is significant in both with a negative fold change in the other time point. The total number of significantly differentially expressed genes with positive or negative fold changes are shown in the top left or bottom left respectively. Genes are abbreviated as follows: FBA fructose-bisphosphate aldolase, FBP1 ferrichrome-binding protein, FLDA flavodoxin, ISIP3 iron-starvation induced protein 3, ZIP ZRT, IRT-like protein. Numbers used for gene annotation correspond to protein IDs in the *E. huxleyi* CCMP1516 genome.

variability in expression between time points increased for mitochondrial GOGAT genes compared to the fairly stable expression in the iron-replete treatment with significant upregulation under low iron at T3 (Figs. 5B and S8). The mitochondrial GOGAT genes are specialized to recover recycled nitrogen and/or assimilate urea (8); therefore, in conjunction with the ammonium and urea transporters being upregulated under low iron, this transcriptional response is consistent with a greater emphasis on utilizing recycled forms of N. As with the lack of change in OUC genes throughout the UCBC, there were no significant differences in OUC transcript abundances between iron treatments at all time points.

Other differentially expressed genes show how *C. decipiens* responds to iron limitation during the UCBC (Fig. 6A, Dataset S6). Similar to other diatoms, several transcriptional indicators of iron stress showed significant upregulation in the iron-limited treatment. Transcripts for the inorganic iron uptake gene phytotransferrin (*pTF*; previously known as *ISIP2a*) were upregulated at all time points in Fe-limited cells ($P < 0.0001$)(16). Flavodoxin (*FLDA*) is an iron-free replacement for the photosynthetic electron transfer protein ferredoxin (58); diatoms can possess multiple copies of *FLDA* with some that are not iron responsive (59). Two copies of *FLDA* were detected, one of which was significantly upregulated at all time points in Fe-limited cells ($P < 0.0001$) and the other was not. A gene encoding for a metacaspase similar to one identified in *T. pseudonana* (*TpMC4*), was significantly upregulated at all time points ($P < 0.0001$); this protein has been implicated in programmed cell death suggesting a triggering of this process in iron-limited cells (60).

Some genes displayed differential expression only at certain time points throughout the UCBC. *ISIP3*, a gene of unknown function normally highly expressed under iron limitation in diatoms, was only upregulated at T1 ($P = 0.06$) and T5 ($P = 0.005$) indicating that this gene may not be a reliable marker for iron stress in *Chaetoceros* under serial or colimitation scenarios unlike *T. oceanica* (56, 61, 62). A ferric reductase in the cytochrome b_5 family was differentially expressed only in the light ($P < 0.001$). This contig is homologous to *FRE3* and *FRE4* in P. tricornutum which are speculated to be involved in heme-based iron uptake (56). Two class I fruc-

tose 1,6-bisphosphate aldolase (*FBA*) contigs were upregulated under low Fe, although one was only upregulated in the light and other in the dark (T3). These enzymes are important for cellular C metabolism and are commonly found to be upregulated in iron-limited diatoms (57, 63).

Three contigs encoding aureochromes were differentially expressed as a function of iron status at certain time points. Aureochromes are light-induced transcription factors specific to stramenopiles (64); all three of these in *C. decipiens* contain the characteristic bZIP domain for DNA binding and the light-oxygen-voltage (LOV) domain for blue-light sensing (65). These proteins have previously been implicated in diel regulation of gene expression (66). None were differentially expressed between iron treatments during exponential growth, only increasing in expression in iron-limited cells when in stationary phase in the dark, suggesting that these have an increased role in regulating gene expression when both N and Fe are limiting, a colimitation scenario which may be commonplace in the ocean (67).

Despite its prevalence and ability to grow under low iron, differential expression in *E. huxleyi* between varied iron treatments has not been analyzed previous to this study. This analysis was restricted to T1 and T2 as only these time points had replicates available (Fig. 6B, Dataset S7). More genes were differentially expressed at T1 compared to T2 (Fig. 6B). Only two contigs showed significant opposing regulation between T1 and T2, that is, one was upregulated at one time point but downregulated at the other.

Many of the genes upregulated under iron limitation were similar to those that have been frequently observed in diatoms. These include the previously mentioned genes *ISIP3*, *FBA Class I*, and *FLDA*. High expression of *FBP1* and ZIP family divalent metal transporters were also detected. FBP1 is involved in siderophore-based Fe uptake in diatoms suggesting a similar functional role in *E. huxleyi* (68). ZIP family transporters may also permit transport of ferrous iron (69). Other highly expressed genes have no annotated function (e.g. *E. huxleyi* CCMP1516 IDs: 103255, 110131, 112797) suggesting that *E. huxleyi* possesses or employs unique mechanisms for coping with iron limitation. These genes and the proteins they encode are clear targets for future study and possible markers of iron stress in *E. huxleyi* in the natural environment.

Conclusions. Phytoplankton in upwelling regions are exposed to highly dynamic conditions as a result of upwelling cycles. In these upwelling cycle simulations, both a representative diatom, *C. decipiens*, and the coccolithophore, *E. huxleyi*, displayed physiological and transcriptional plasticity to these cycles. Part of this physiological response included transitioning to high cellular C:N ratios which has previously been observed in natural populations and influences the biogeochemical cycling of these elements. Although both phytoplankton species were transcriptionally responsive, their gene expression patterns at each time point was highly divergent. In particular, *C. decipiens* exhibited a pattern of frontloading transcriptional and nitrate assimilation genes, which may explain certain diatoms' ability to rapidly respond and outcompete other groups once upwelling events occur. Previous studies, however, indicate a disconnect between nitrate assimilation transcripts and protein abundances in diatoms, and it is possible that the frontloading response may not result in the synthesis of mature proteins (70, 71).

As a highly diverse group, diatoms likely occupy a wide range of niches and growth strategies (19). The response characterized here may be relatively exclusive to bloom-forming diatoms in upwelling regions although transcriptional responses in nitrate assimilation genes appear fairly consistent among diatoms in the laboratory studies. Furthermore, it is likely even among bloom-forming diatoms that there are further divergences in the transcriptional responses as observed in a previous field simulation (6).

Both *C. decipiens* and *E. huxleyi* appear to employ mechanisms in response to iron stress that are common to responses previously observed in diatoms; however, certain genes such as aureochromes appear to only be differentially expressed when N and/or light is simultaneously limiting, indicating a unique response under colimitation scenarios. In *E. huxleyi*, many of the genes that were differentially expressed are not functionally characterized. Importantly, *E. huxleyi* was unable to respond to prolonged darkness under iron-limiting conditions whereas *C. decipiens*'s shift-up response once returned to the light was unaffected. Some projections suggest increased iron limitation in upwelling environments as a result of ocean acidification and increases in upwelled nitrate relative to iron (1, 16); however, these findings suggest that diatoms will continue to exhibit the shift-up response and outcompete other phytoplankton groups under both high and low iron upwelling conditions.

ACKNOWLEDGEMENTS

We thank Liah McPherson, Jackie Millay, and Sharla Sugierski for assistance with the culture experiments and sample processing. This work was funded by National Science Foundation grants DGE-1650112, DGE-1650116 (Graduate Research Fellowship to R.H.L), OCE-1751805 (to A.M.), and ICER-1600506 (stipend for G.H.). Funding for sequencing was also provided by a Phycological Society of America Grant-in-Aid of Research (to. R.H.L.).

CONFLICT OF INTERESTS

The authors have no conflict of interests.

References

1. Capone DG, Hutchins DA (2013) Microbial biogeochemistry of coastal upwelling regimes in a changing ocean. *Nature Geosci* 6(9):711–717.
2. Wilkerson FP, Dugdale RC (2008) *Nitrogen in the Marine Environment (2nd Edition).* (Academic Press, Burlington, MA, USA).
3. MacIsaac JJ, Dugdale RC, Barber RT, Blasco D, Packard TT (1985) Primary production cycle in an upwelling center. *Deep-Sea Res* 32(5):503–529.
4. Wilkerson FP, Dugdale RC (1987) The use of large shipboard barrels and drifters to study the effects of coastal upwelling on phytoplankton dynamics. *Limnol Oceanogr* 32(2):368–382.
5. Estrada M, Blasco D (1985) *Phytoplankton assemblages in coastal upwelling areas*, eds. Bas C, Margalef R, Rubies P. (Barcelona) Vol. 1, pp. 379–402.
6. Lampe RH, et al. (2018) Divergent gene expression among phytoplankton taxa in response to upwelling. *Environ Microbiol* 20:3069–3082.
7. Fawcett S, Ward B (2011) Phytoplankton succession and nitrogen utilization during the development of an upwelling bloom. *Mar Ecol-Prog Ser* 428:13–31.
8. Smith SR, et al. (2019) Evolution and regulation of nitrogen flux through compartmentalized metabolic networks in a marine diatom. *Nat Commun* 10(1):4552.
9. Kudela RM, Dugdale RC (2000) Nutrient regulation of phytoplankton productivity in monterey bay, california. *Deep-Sea Res Pt II* 47(5-6):1023–1053.
10. Bruland KW, Rue EL, Smith GJ, DiTullio GR (2005) Iron, macronutrients and diatom blooms in the peru upwelling regime: brown and blue waters of peru. *Mar Chem* 93(2-4):81–103.
11. Bruland KW, Rue EL, Smith GJ (2001) Iron and macronutrients in california coastal upwelling regimes: Implications for diatom blooms. *Limnol Oceanogr* 46(7):1661–1674.

12. Hutchins DA, DiTullio GR, Zhang Y, Bruland KW (1998) An iron limitation mosaic in the california upwelling regime. *Limnol Oceanogr* 43(6):1037–1054.
13. Hutchins D, et al. (2002) Phytoplankton iron limitation in the humboldt current and peru upwelling. *Limnol Oceanogr* 47(4):997–1011.
14. Till CP, et al. (2019) The iron limitation mosaic in the california current system: factors governing iron availability. *Limnol Oceanogr* 64(1):109–123.
15. Bakun A (1990) Global climate change and intensification of coastal ocean upwelling. *Science* 247(4939):198–201.
16. McQuaid JB, et al. (2018) Carbonate-sensitive phytotransferrin controls high-affinity iron uptake in diatoms. *Nature* 555:534.
17. Shi D, Xu Y, Hopkinson BM, Morel FMM (2010) Effect of ocean acidification on iron availability to marine phytoplankton. *Science* 327(5966):676–679.
18. Lampe RH, et al. (year?) The distribution and diversity of diatoms in a coastal upwelling biome in *Ocean Sciences Meeting*.
19. Malviya S, et al. (2016) Insights into global diatom distribution and diversity in the world's ocean. *Proc Natl Acad Sci USA* 113(11):E1516–E1525.
20. Read BA, et al. (2013) Pan genome of the phytoplankton emiliania underpins its global distribution. *Nature* 499:209.
21. Venrick EL (2012) Phytoplankton in the california current system off southern california: Changes in a changing environment. *Prog Oceanogr* 104:46–58.
22. Ziveri P, Thunell RC, Rio D (1995) Export production of coccolithophores in an upwelling region: Results from san pedro basin, southern california borderlands. *Mar Micropaleontol* 24(3):335–358.
23. Marchetti A, Catlett D, Hopkinson BM, Ellis K, Cassar N (2015) Marine diatom proteorhodopsins and their potential role in coping with low iron availability. *ISME J* 9:2745.
24. Price NM, et al. (1989) Preparation and chemistry of the artificial algal culture medium aquil. *Biol Oceanogr* 6:443–461.
25. Sunda WG, Price NM, Morel FM (2005) Trace metal ion buffers and their use in culture studies. *Algal culturing techniques* 4:35–63.
26. Brand LE (1985) Low genetic variability in reproduction rates in populations of prorocentrum micans ehrenb. (dinophyceae) over georges bank. *J Exp Mar Biol Ecol* 88(1):55–65.
27. Meyer E, Aglyamova GV, Matz MV (2011) Profiling gene expression responses of coral larvae (acropora millepora) to elevated temperature and settlement inducers using a novel rna-seq procedure. *Mol Ecol* 20(17):3599–3616.
28. Lohman BK, Weber JN, Bolnick DI (2016) Evaluation of tagseq, a reliable low-cost alternative for rnaseq. *Mol Ecol Resour* 16(6):1315–1321.
29. Strader ME, Aglyamova GV, Matz MV (2016) Red fluorescence in coral larvae is associated with a diapause-like state. *Mol Ecol* 25(2):559–569.
30. Dixon GB, et al. (2015) Genomic determinants of coral heat tolerance across latitudes. *Science* 348(6242):1460–1462.
31. Bolger AM, Lohse M, Usadel B (2014) Trimmomatic: A flexible trimmer for illumina sequence data. *Bioinformatics* 30(15):2114–2120.
32. Patro R, Duggal G, Love MI, Irizarry RA, Kingsford C (2017) Salmon provides fast and bias-aware quantification of transcript expression. *Nat Meth* 14(4):417–419.
33. Love MI, Huber W, Anders S (2014) Moderated estimation of fold change and dispersion for rna-seq data with deseq2. *Genome Biol* 15(12):550.
34. Langfelder P, Horvath S (2008) Wgcna: an r package for weighted correlation network analysis. *BMC Bioinform* 9(1):559.
35. Benjamini Y, Hochberg Y (1995) Controlling the false discovery rate: A practical and powerful approach to multiple testing. *J R Stat Soc B* 57(1):289–300.
36. Liefer JD, et al. (2019) The macromolecular basis of phytoplankton c:n:p under nitrogen starvation. *Front Microbiol* 10(763).
37. Hutchins DA, Bruland KW (1998) Iron-limited diatom growth and si:n uptake ratios in a coastal upwelling regime. *Nature* 393(6685):561–564.
38. Schnetzer A, et al. (2017) Marine snow formation by the toxin-producing diatom, pseudo-nitzschia australis. *Harmful Algae* 61:23–30.
39. Wong CM, Kewu P, Zhe H, Lee J (2015) Current perspectives on the role of tramp in nuclear rna surveillance and quality control. *Research and Reports in Biochemistry* 2015:111.
40. Barshis DJ, et al. (2013) Genomic basis for coral resilience to climate change. *P Natl Acad Sci USA* 110(4):1387–1392.
41. McKew BA, Metodieva G, Raines CA, Metodiev MV, Geider RJ (2015) Acclimation of emiliania huxleyi (1516) to nutrient limitation involves precise modification of the proteome to scavenge alternative sources of n and p. *Environ Microbiol* 17(10):4050–4062.
42. Allen AE, et al. (2011) Evolution and metabolic significance of the urea cycle in photosynthetic diatoms. *Nature* 473(7346):203–207.
43. Rokitta SD, Von Dassow P, Rost B, John U (2014) Emiliania huxleyi endures n-limitation with an efficient metabolic budgeting and effective atp synthesis. *BMC genomics* 15(1):1051–1051.
44. Alipanah L, Rohloff J, Winge P, Bones AM, Brembu T (2015) Whole-cell response to nitrogen deprivation in the diatom phaeodactylum tricornutum. *J Exp Bot* 66(20):6281–6296.
45. Bender S, Durkin C, Berthiaume C, Morales R, Armbrust EV (2014) Transcriptional responses of three model diatoms to nitrate limitation of growth. *Front Mar Sci* 1(3).
46. Kang LK, Rynearson TA (2019) Identification and expression analyses of the nitrate transporter gene (nrt2) family among skeletonema species (bacillariophyceae). *J Phycol* 55(5):1115–1125.
47. Alexander H, Rouco M, Haley ST, Dyhrman ST (in press) Transcriptional response of emiliania huxleyi under changing nutrient environments in the north pacific subtropical gyre. *Environmental Microbiology*.
48. Kaffes A, et al. (2010) Carbon and nitrogen fluxes in the marine coccolithophore emiliania huxleyi grown under different nitrate concentrations. *J Exp Mar Biol Ecol* 393(1):1–8.
49. Rouco M, Branson O, Lebrato M, Iglesias-Rodríguez MD (2013) The effect of nitrate and phosphate availability on emiliania huxleyi (nzeh) physiology under different co2 scenarios. *Front Microbiol* 4:155.
50. Deutsch C, et al. (2020) Biogeochemical variability in the california current system. *bioRxiv* p. 2020.02.10.942565.
51. Hogle SL, et al. (2018) Pervasive iron limitation at subsurface chlorophyll maxima of the california current. *Proc Nat Acad Sci USA* 115(52):13300–13305.
52. Sutak R, et al. (2012) A comparative study of iron uptake mechanisms in marine microalgae: Iron binding at the cell surface is a critical step. *Plant Physiol* 160(4):2271–2284.
53. Cermeño P, Lee JB, Wyman K, Schofield O, Falkowski PG (2011) Competitive dynamics in two species of marine phytoplankton under non-equilibrium conditions. *Mar Ecol Prog Ser* 429:19–28.
54. Morel FMM, Hudson RJM, Price NM (1991) Limitation of productivity by trace metals in the sea. *Limnol Oceanogr* 36(8):1742–1755.
55. Raven JA (1988) The iron and molybdenum use efficiencies of plant growth with different energy, carbon and nitrogen sources. *New Phytol* 109(3):279–287.
56. Allen AE, et al. (2008) Whole-cell response of the pennate diatom phaeodactylum tricornutum to iron starvation. *P Natl Acad Sci USA* 105(30):10438–43.
57. Cohen NR, et al. (2017) Variations in diatom transcriptional responses to changes in iron availability across ocean provinces. *Front Mar Sci* 4:360.
58. La Roche J, Geider RJ, Graziano LM, Murray H, Lewis K (1993) Induction of specific proteins in eukaryotic algae grow under iron-, phosphorus-, or nitrogen-deficient conditions. *J Phycol* 29(6):767–777.
59. Whitney L, et al. (2011) Characterization of putative iron responsive genes as species-specific indicators of iron stress in thalassiosiroid diatoms. *Front Microbiol* 2(234).
60. Bidle KD, Bender SJ (2008) Iron starvation and culture age activate metacaspases and programmed cell death in the marine diatom thalassiosira pseudonana. *Eukaryot Cell* 7(2):223–236.
61. Chappell PD, et al. (2015) Genetic indicators of iron limitation in wild populations of thalassiosira oceanica from the northeast pacific ocean. *ISME J* 9(3):592–602.
62. Cohen NR, et al. (2017) Iron and vitamin interactions in marine diatom isolates and natural assemblages of the northeast pacific ocean. *Limnol Oceanogr* 62:2076–2096.
63. Allen AE, et al. (2012) Evolution and functional diversification of fructose bisphosphate aldolase genes in photosynthetic marine diatoms. *Mol Biol Evol* 29(1):367–379.
64. Kroth PG, Wilhelm C, Kottke T (2017) An update on aureochromes: Phylogeny – mechanism – function. *J Plant Physiol* 217:20–26.
65. Takahashi F, et al. (2007) Aureochrome, a photoreceptor required for photomorphogenesis in stramenopiles. *P Natl Acad Sci USA* 104(49):19625–19630.
66. Goldman JAL, et al. (2019) Fe limitation decreases transcriptional regulation over the diel cycle in the model diatom thalassiosira pseudonana. *PLOS ONE* 14(9):e0222325.
67. Browning TJ, et al. (2017) Nutrient co-limitation at the boundary of an oceanic gyre. *Nature* 551(7679):242–246.
68. Coale TH, et al. (2019) Reduction-dependent siderophore assimilation in a model pennate diatom. *Proc Natl Acad Sci USA* 116(47):23609–23617.
69. Eide DJ (2005) *The Zip Family of Zinc Transporters*, eds. Iuchi S, Kuldell N. (Springer US, Boston, MA), pp. 261–264.
70. Hockin NL, Mock T, Mulholland F, Kopriva S, Malin G (2012) The response of diatom central carbon metabolism to nitrogen starvation is different from that of green algae and higher plants. *Plant Physiol* 158(1):299–312.
71. Poulsen N, Kröger N (2005) A new molecular tool for transgenic diatoms. *FEBS J* 272(13):3413–3423.